Applied Surface Science Advances 18 (2023) 100473

Contents lists available at ScienceDirect

Applied Surface Science Advances

journal homepage: www.sciencedirect.com/journal/applied-surface-science-advances

Defective cobalt and copper tungstates mixtures with TiO_2 for photocatalytic CO_2 reduction

Kamil Urbanek [a,b], Anna Jakimińska [a,b], Kaja Spilarewicz [a], Wojciech Macyk [a,*]

[a] Faculty of Chemistry, Jagiellonian University, ul. Gronostajowa 2, Kraków 30-387, Poland
[b] Doctoral School of Exact and Natural Sciences, Jagiellonian University, ul. S. Łojasiewicza 11, Kraków 30-348, Poland

ARTICLE INFO

Keywords:
Tungstates
Photocatalysis
CO_2 reduction
Titanium dioxide
Defects

ABSTRACT

In this work, the application of highly defective cobalt and copper tungstates was proposed for photocatalytic CO_2 reduction. The materials were synthesized by hydrothermal method and characterized with SEM, EDS, XRD, XPS and DRS techniques. Studied materials were examined in photocatalytic CO_2 reduction to CO in the gas phase, as bare photocatalysts and in mixtures with TiO_2. The behavior of the junctions between the mixture components was determined using photoelectrochemical, spectroelectrochemical and surface photovoltage measurements. These studies reveal different types of junctions for the synthesized materials (disturbed S-scheme for CoT/TiO_2 and type-I for CuT/TiO_2). It was found the CuT/TiO_2 mixture is more effective than CoT/TiO_2 due to lower recombination rates of photogenerated charge carriers and the presence of a larger number of W^{5+} and Cu^{2+} active centers.

Introduction

Photocatalytic reduction of CO_2 is a promising solution to the growing CO_2 problem which allows for its transformation into valuable fuels or chemicals using sunlight as the energy source. Researchers work on developing efficient and robust photocatalysts, that can harness solar energy to drive the conversion of CO_2, thereby reducing greenhouse gas emissions and, therefore, the effects of climate change. Improved materials with enhanced light absorption, charge separation, and catalytic activity are crucial for achieving high conversion rates and selectivity, making the search for better materials a critical avenue of research in our quest for sustainable and renewable energy solutions.

Tungsten oxide is a well-known material in photocatalysis [1–3], however, it was found that the pristine material is scarcely active in CO_2 reduction [4,5]. Nevertheless, the presence of unoccupied *d* orbitals in transition metals may activate the CO_2 molecule, *e.g.*, by an adduct formation [6]. Several studies confirmed that tungstate anion serves as a homogeneous catalyst for CO_2 fixation, forming carbamic acid [7,8], which indicates that tungsten can be recognized as an active site for CO_2 chemical transformations.

It was found that in contrast to the bare tungsten oxide its hydrated form, $WO_3 \bullet 0.33H_2O$, is effective as the photocatalyst for CO_2 reduction to CH_4 [9] and acetate [10]. The photocatalytic performance of the material can be affected by the presence of W^{5+} and, therefore, oxygen vacancies [10,11]. Oxygen vacancies are reported *inter alia* to promote charge separation in the Z-scheme [12] and are considered the active sites for CO_2 bonding [13,14]. Such defects can be engineered by the control of the synthesis conditions, *e.g.*, the solution pH, as the tungstates anions can exist in various forms [15] which can affect the uniform crystal growth [16].

The hydrated form of tungsten oxide, $WO_3 \bullet H_2O$, can be formally considered as tungstic acid H_2WO_4. However, the acid is not highly stable, their salts *e.g.*, Na_2WO_4, $CaWO_4$, and $CdWO_4$ are known for decades [17,18]. Transition divalent metal tungstates with a general formula $M^{2+}WO_4$ (M^{2+} = Cd, Cu, Co, Mn and Ni *etc.*) constitute an interesting class of photocatalysts offering exceptional optical and electronic features. Many tungstates are attractive owing to their low cost, high stability, narrow band gap, and easy operation [19]. The presence of accompanying metal induces changes in the electronic structure of the tungstate when compared to WO_3 [20]. Moreover, the selection of metals introduces various active sites for particular chemical reactions and enables bandgap engineering, as a consequence of mixing of the M *s*-orbitals and O 2*p*-orbitals [21,22]. These factors are crucial for tailoring photocatalytic and electronic properties of tungstates. This was proved so far for such applications as hydrogen evolution [23–25] and photocatalytic oxidation of organics [26,27]. In recent literature, there

* Corresponding author.
E-mail address: macyk@chemia.uj.edu.pl (W. Macyk).

https://doi.org/10.1016/j.apsadv.2023.100473
Received 8 August 2023; Received in revised form 9 October 2023; Accepted 11 October 2023
Available online 19 October 2023

has been a growing interest in the application of these materials. In particular, reports on the use of $CoWO_4$ and $CuWO_4$ in CO_2 reduction appeared [28,29].

The cobalt tungstate ($CoWO_4$) with a bandgap of 2.2 to 2.8 eV [19,25,30] is known for its great optical, electrical and magnetic properties [19,30,31], and the copper tungstate is an *n*-type semiconductor photocatalyst [32,33] which has advantageous optical properties due to its bandgap (2.2–2.4 eV) [32–37]. Moreover, copper tungstate, depending on the synthesis conditions, can crystallize in the form of copper tungstate hydrates or other mixed phases. These forms are obtained most often during precipitation synthesis [38–42]. Among them, copper tungstate hydroxide is a very sparsely studied material. One publication by Sahdost-Fard et al. describes its application in the aptasensing of bacteria [43]. Another one indirectly mentions the material as a precursor of $CuWO_4$ and describes its use in phenol degradation [44].

The efficiency of photocatalytic processes relies *inter alia* on the ability of the material to absorb light, separate charges efficiently and transfer them *via* redox reactions toward substrates. It is difficult to develop a single-component semiconductor with all of the required properties, which is often raised in the literature, and thus this is the cause for a plethora of investigations into different strategies to optimize the materials [45]. The main disadvantage of bare tungsten oxides in photocatalysis is their high charge recombination rate, but this problem can be overcome by the addition of a co-catalyst [46] or by creating a heterojunction [19,47]. Another solution is to create S-scheme systems by, for example, combining tungstates with TiO_2 [48–51].

To the best of our knowledge, there are no reports of photocatalytic CO_2 reduction in the gas phase with H_2O as a hole scavenger on the mixtures of copper or cobalt tungstate with TiO_2. In this work, the cobalt tungstate (denoted as CoT) and copper tungstate hydroxide (denoted as CuT) were synthesized and combined with TiO_2 anatase for a gas phase photocatalytic CO_2 reduction to CO, and the mechanisms of these processes were examined. It was found that one of the studied tungstates combined with TiO_2 formed a disturbed S-scheme, while the other produced a type-I heterojunction. This allowed for the comparison of these two strategies and the determination of the factors that influence the efficiency of the formed junctions.

Experimental

Reagents

Copper(II) nitrate hemi(pentahydrate) $Cu(NO_3)_2{\bullet}5H_2O$ (Sigma-Aldrich, 98%), cobalt nitrate hexahydrate $Co(NO_3)_2{\bullet}6H_2O$ (Chempur, pure), sodium tungstate $Na_2WO_4{\bullet}2H_2O$ (Merck, for analysis), sodium hydroxide NaOH (POCh, pure), and TiO_2 anatase powder (TRONOX, AK-1) were used without further purification. Deionized H_2O was obtained using a Hydrolab system (HLP 10UV, 0.05 μS, $t = 20$ °C).

Synthesis of studied materials

Copper and cobalt tungstates were obtained through the precipitation method followed by hydrothermal treatment.

In typical synthesis 0.001 mol of $Cu(NO_3)_2{\bullet}5H_2O$ or $Co(NO_3)_2{\bullet}6H_2O$ was dissolved in 20 ml of deionized (DI) H_2O. At the same time, 0.001 mol of sodium tungstate was dissolved in another 20 ml of deionized H_2O and added dropwise to the previously prepared precursor solution. The reaction mixtures were stirred for 20 min, and their pH was adjusted to 8 with an aqueous NaOH solution. Obtained precipitates were heated to 180 °C for 12 h in Teflon-lined autoclaves and then, left to cool down to room temperature. Then, the products were washed several times with deionized H_2O to neutralize the pH and remove post-synthetical impurities.

Preparation of mixtures with TiO_2

The mixtures of synthesized materials were obtained by simply mixing and grinding the sample with TiO_2 in an agate mortar in a 1:1 wt ratio.

DRS

The Tauc method described by Makuła *et al.* [52] was used to estimate the bandgap of materials. Diffuse reflectance (DRS) spectra were recorded and transformed using Kubelka-Munk and Tauc functions. The measurements were performed with a Shimadzu UV-3600 UV–Vis-NIR spectrophotometer equipped with a 10 cm dia. integrating sphere, and pure $BaSO_4$ was used as a reference. The samples were mixed with $BaSO_4$ in quantities determined by the strength of the reflectance signal.

SEM and EDS

SEM micrographs were obtained on Helios 5 Hydra DualBeam, using TLD in immersion mode. EDS analysis was performed using Tescan Vega 3 microscope and Oxford Instruments detector (X-act, SDD 10 mm^2).

XRD

X-ray diffractometer (XRD) Rigaku MiniFlex (PANalytical) with nickel-filtered copper K_α radiation ($\lambda = 0.15406$ nm, 40 kV, 15 mA) was applied to study the crystalline structure of the powder materials. Data were recorded in the range of $2\theta = 10$–$90°$ with 0.02° step at a scan rate of 2°/min. Analysis was performed using QualX software [53] and the POW_COD database [54–57].

XPS

To determine surface compositions and oxidation states of copper and cobalt tungstates X-ray photoelectron spectroscopy measurements were performed with a Prevac photoelectron spectrometer with a hemispherical VG Scienta R3000 analyser (100 eV energy pass), using the Al K_α ($\lambda = 1486.6$ eV) radiation source, and the background pressure in the analysis chamber was 10^{-8} mbar. Static charging of the samples was corrected by shifting binding energies to match the C 1 s peak of adventitious carbon peak to 248.8 eV.

SPV

Differences in the contact potential difference (CPD) of the sample irradiated with intermittent light were measured on an environmental Kelvin probe (Instytut Fotonowy) to obtain surface photovoltage. The electrode with respect to which the potential was measured was the Au 2.5 mm diameter mesh. A xenon lamp with a monochromator was used as the light source.

Photoelectrochemical measurements

To measure the transient photocurrents [58], the three-electrode cell with potentiostat, 150 W xenon lamp and monochromator, supplied by Instytut Fotonowy, was used. The electrodes were: the working electrode – a thin layer of studied material spread on a transparent ITO foil (60 Ω/sq, Sigma-Aldrich); counter electrode – Pt wire; reference electrode – Ag/AgCl electrode with 3 M KCl electrolyte. The cell electrolyte – 0.1 M KNO_3 – was purged with Ar during and before the experiment.

Spectroelectrochemical measurements

The density of states measurements were performed using a Shimadzu UV-3600 spectrophotometer and BioLogic SP-150 potentiostat. In the experiment, DRS spectra were measured for different potentials applied in a three-electrode cell with Ag/Ag^+ reference electrode (0.01 M $AgNO_3$ and 0.1 M TBAP in ACN), Pt wire counter electrode, and Pt foil

covered with the examined material working electrode. The potential step between each DRS measurement was 50 mV with 20 min equilibration time and the range of applied potentials was 0 to –2.7 V *vs.* reference electrode. A solution of $LiClO_4$ 0.1 M in acetonitrile was used as an electrolyte. The resulting graph depicts differences in the Kubelka-Munk function for a selected wavelength between the two following potentials *vs.* applied potential.

Photocatalytic activity

To study the photocatalytic activity in CO_2 reduction in the gas phase, a thin layer of the studied material (15 mg) was spread on a glass plate (4 cm^2) and placed in a glass test tube (13 ml) covered with a silicone septum cap. The reactor atmosphere was CO_2 in Ar in the ratio of 1:5 saturated with H_2O vapor (from 340 µl of DI H_2O purged with Ar placed on the bottom of the tube) at ambient pressure. The reactor was irradiated by light from a 150 W xenon lamp light passing through a 100 mm H_2O filter (300 mW/cm^2). The glass material of the tube absorbs below 340 nm. The temperature remained at 36 °C throughout the experiment. Gas from the reactor was sampled with a 50 µl syringe and then analyzed with Thermo-Scientific Trace 1300 gas chromatograph equipped with a methanizer (Restek), FID and TCD detectors and Carboxen 1010 column for methane, ethane, carbon monoxide, CO_2, and air analysis. Ultra-pure (ppm level of impurities) Ar from Air Products was used as the carrier gas. The CO_2 reduction to CO was proved by the blank experiments (*i.e.*, without CO_2). All experimental series were blank-corrected. For more details please see Supporting Information.

To confirm the H_2O oxidation to hydroxyl radicals, experiments with terephthalic acid were carried out. In these tests, 12 mg of a CoT, CuT or TiO_2 was suspended in 12 ml of the 3 mM terephthalic acid (TA) and 0.1 M NaOH mixture and was irradiated by the same light source setup as in the aforementioned experiment of CO_2 reduction with the use of Xe lamp. Samples were taken every 10 min for 60 min and the fluorescence spectra were recorded using a Perkin Elmer LS-55 fluorimeter (λ_{ex} = 315 nm). The hydroxyterephthalic acid (TAOH) formation was monitored as the increase of the maximum at 425 nm.

Results and discussion

Solvothermal synthesis is a common approach for obtaining crystalline materials, however, solvents or other agents used are often organic. If the obtained product is not properly purified, the remaining carbon may produce false results in photocatalytic tests of CO_2 reduction. Therefore, the hydrothermal synthesis of cobalt tungstate (CoT) and copper tungstate (CuT), in which the carbon-free inorganic substrates were used, was selected. The syntheses resulted in dark violet CoT and bright green CuT solids. Obtained materials were purified and subsequently characterized. The materials were further ground with commercial TiO_2 (anatase phase) to form the junctions and their behavior in photocatalytic processes was examined. The commercial TiO_2 was selected to avoid the post-synthetic impurities. This helped to ensure that the carbon in the product of photocatalytic CO_2 reduction does not come from any other undesired side process.

SEM

The morphology of obtained materials was examined using SEM revealing agglomerated nanoparticles (Fig. 1). Synthesized CoT forms nanorods with an average dimension in the longitudinal axis in the range of 15–150 nm and *ca.* 15 nm in the transverse direction. A similar morphology of $CoWO_4$ obtained by the hydrothermal method was reported by Zhen et al. [59]. CuT exhibits a polygonal structure resulting from the aggregation of fine nanoparticles. The average diameter of formed nanoparticles is *ca.* 25 nm.

Additionally, EDS analysis confirmed the presence of the constituent elements in both materials (**Fig. S2**). For CoT, the approximate atomic ratio of Co to W was 1 to 1 and for CuT the ratio of Cu to W was 2 to 1.

XRD

The XRD patterns of both materials (Fig. 2) exhibit the peaks widening indicating the formation of small crystallites. From the Scherrer equation, an average crystallite size of 13 and 12 nm was estimated for CoT and CuT respectively. The diffractogram of TiO_2 anatase is presented in **Fig. S3.**

The diffractogram of obtained CoT corresponds with the JCPDS card 15–0867 ($CoWO_4$). All peaks match closely with only slightly shifted positions. This shows that the material may exhibit some irregularities in the crystal lattice caused most likely by the small crystallite size.

The diffractogram of obtained CuT reveals peaks characteristic of

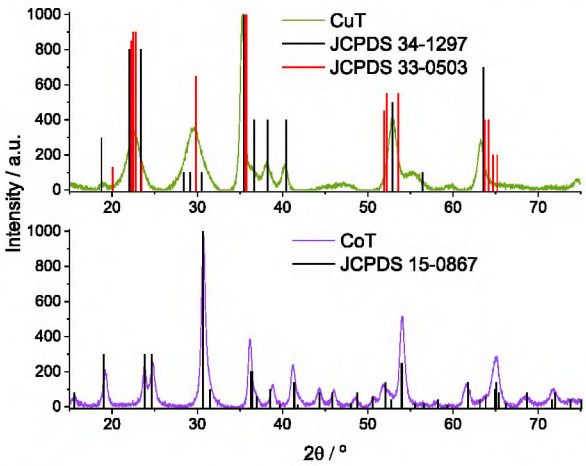

Fig. 2. XRD diffractograms of obtained materials. Intensities were normalized.

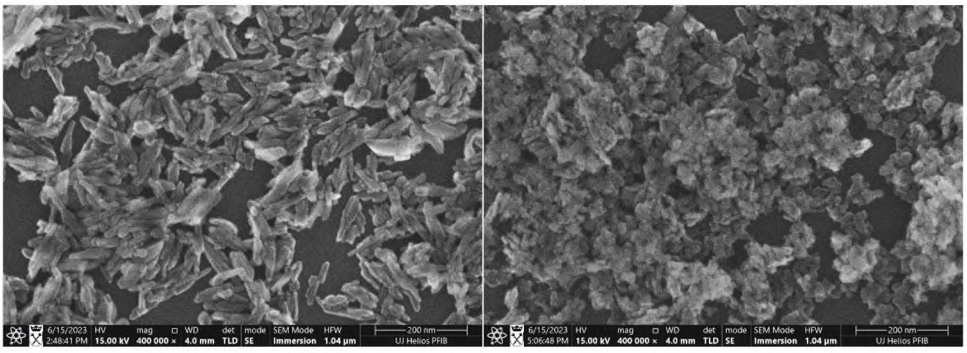

Fig. 1. SEM micrographs of CoT (left) and CuT (right).

both $CuWO_4{\cdot}2H_2O$ (JCPDS card 33-0503) and $Cu_2WO_4(OH)_2$ (JCPDS card 034–1297) phases. Both materials, when the particles are of sufficiently small diameters, may exhibit similar diffractograms as reported by Cheng [60] and Souza et al. [61]. Precipitation of the material from the basic solution of WO_4^{2-} and Cu^{2+} ions might result in the formation of both $CuWO_4{\cdot}2H_2O$ and $Cu_2WO_4(OH)_2$ [38]. Peaks of these two phases lie mostly at the same positions, excluding the peaks at 19°, 38°, and 40° characteristic of the second phase. The presence of these peaks in the diffractogram of synthesized material (marked with asterisks) confirms the existence of the $Cu_2WO_4(OH)_2$ phase. Moreover, the $Cu_2WO_4(OH)_2$ phase exists as the cuprotungstite mineral [62] which has a green color, whilst pristine $CuWO_4$ is pale yellow or amber [63]. Thus, the color of obtained material corroborates with the color of the mineral indicating the presence of the mentioned phase.

XPS

X-ray photoelectron spectroscopy was used to analyze the oxidation states of elements in CoT and CuT (Fig. 3Fig. 4). Deconvoluted W $4f_{7/2}$ and $4f_{5/2}$ region of both materials shows two doublets of peaks characteristic of W^{5+} and W^{6+} species, respectively [64,65]. This confirms the presence of expected W^{5+} centers in the materials which are supposed to be advantageous for CO_2 adsorption and reduction.

For CoT the Co $2p_{3/2}$ and $2p_{1/2}$ signals are present at binding energies of 781 and 797 eV and are separated by 16 eV characteristic of Co^{2+}, which excludes the presence of Co^{3+} in the sample (Fig. 3) [66]. Furthermore, strong shakeup satellites are present in the spectrum, characteristic of $CoWO_4$ samples [67]. In the W line, two doublets were observed at 34.4 and 36.0 eV. The presence of W^{5+} in this material may be correlated with oxygen defects, as the XPS spectrum of O 1 s depicts a significant peak at 531.7 eV characteristic of defects and OH groups along with the main lattice oxygen peak at 530.0 eV.

The XPS survey spectrum of CuT (**Fig. S4**) shows the Cu to W ratio of 2:1 which points to the presence of the $Cu_2WO_4(OH)_2$ phase in the synthesized material which is in good agreement with the XRD and EDS results.

For the CuT sample, the Cu 2*p* spectrum consists only of Cu^{2+} as evidenced by the strong satellite peak in the vicinity of the $2p_{3/2}$ peak (Fig. 4). The W $4f_{7/2}$ and $4f_{5/2}$ region in this case also shows two doublets of peaks at 34.4 and 35.6 eV indicating the presence of W^{5+} and W^{6+} species, respectively. The presence of W^{5+} may be related to the oxygen defects and OH groups, as the XPS spectrum of O 1 s depicts both the peak at 531.9 eV, characteristic of OH groups and defects, and the main lattice oxygen peak at 530.5 eV. However, in comparison to CoT, in CuT the W^{5+} species constitutes the majority of tungsten. It may result from the synthesis conditions, as the initial solution of copper nitrate was more acidic than the cobalt nitrate. Therefore, more $[W_2O_7(OH)]^{3-}$ ions could have been formed after the addition of sodium tungstate before alkalization, and more OH groups could have been inserted into the structures, as WO_4^{2-} ions are prevalent in pH above 9 [15].

DRS

DRS measurements allowed for the estimation of optical bandgaps of the synthesized materials (**Figs. S5** and Fig. 5). The values were estimated using the Tauc approach, and the transformation for the indirect transition was applied [68]. The indirect gaps were more suitable as they matched the absorption edges energy (**Fig. S5**). Obtained values are 2.66 eV for CoT, and 2.30 eV for CuT indicating absorption in the UV and visible light range (Fig. 5).

Photocurrents

To understand the photoactivity of the bare materials and possible changes in combination with TiO_2, the photocurrent response was measured (Fig. 6). For TiO_2, a strong anodic photocurrent (which informs about the oxidative properties, particularly useful for H_2O oxidation) appears in the whole range of applied potentials within the material absorption range. For bare CoT, the photocurrents are very weak which may indicate fast recombination of photogenerated charge carriers. The photocurrents are anodic in the range of positive potentials, whereas below zero, the response is cathodic (which shows the ability of the material to reduce species present in the electrolyte solution, *e.g.*, CO_2). The spectral range of photocurrent generation by these materials corresponds with the absorption range determined using DRS (compare SI). For CuT, its photoresponse matches the absorption edge, although the photocurrents are anodic in the whole potential range. Moreover, the currents above 400 nm are very weak, indicating not efficient charge separation in this range. After combining the synthesized materials with TiO_2, the photoresponse changed. The change is more pronounced in the case of CuT than CoT. For CoT, the change is visible as the decrease in anodic photocurrent in the range of –100 to 200 mV, whereas in the case of CuT, the cathodic photocurrents emerge in the negative potentials range after mixing with TiO_2. Therefore, the formation of heterojunctions between the synthesized materials and TiO_2 can be assumed.

Photocatalytic activity

Mixtures of the synthesized materials and TiO_2 were examined in the photocatalytic CO_2 reduction in the gas phase. Fig. 7 depicts plots of CO evolution during the tests. In both cases, the activity in CO production is enhanced compared to the activity of bare TiO_2 and bare tungstates. TiO_2 is known for its photocatalytic efficiency, however, its activity in CO_2 reduction is not very impressive. Synthesized bare materials are active in the reduction process, but in comparison to TiO_2, CoT exhibits lower yields of CO evolution. Li et al. reported that a low photoactivity of pristine $CoWO_4$ in CO_2 reduction can be enhanced in the presence of an electron donor and photosensitizer ($[Ru(bpy)_3]^{2+}$, bpy = 2,2′-bipyridine) [28]. Therefore, to improve CoT performance, it should be combined with another photo- or redox-active material. When CuT or CoT are combined with TiO_2, the photoactivity increases, which confirms the

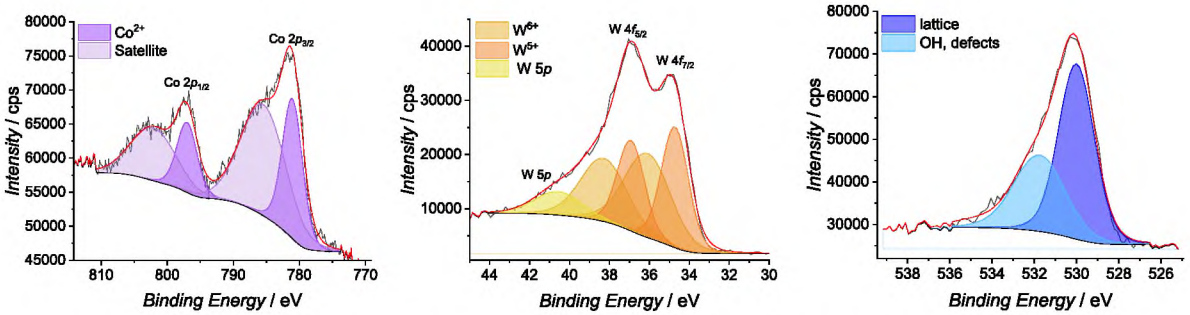

Fig. 3. XPS spectra of Co 2*p*, W 4*f* and O 1 s regions of CoT sample.

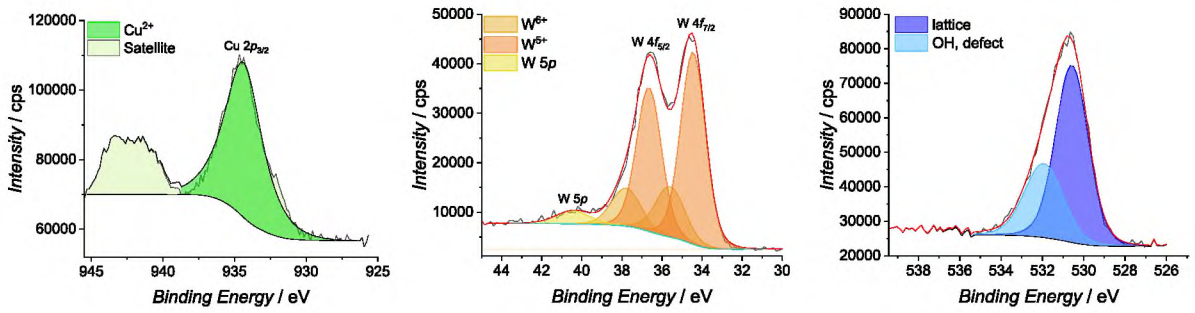

Fig. 4. XPS spectra of Cu 2*p*, W 4*f*, O 1 s regions of CuT sample.

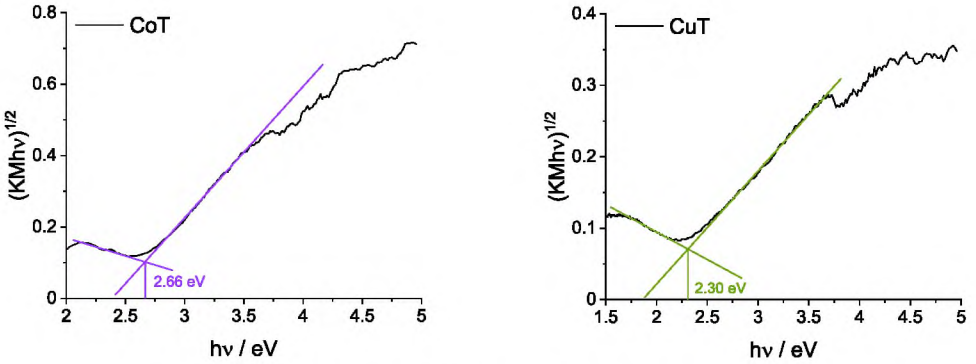

Fig. 5. Tauc plots for CoT and CuT samples for indirect bandgap estimations.

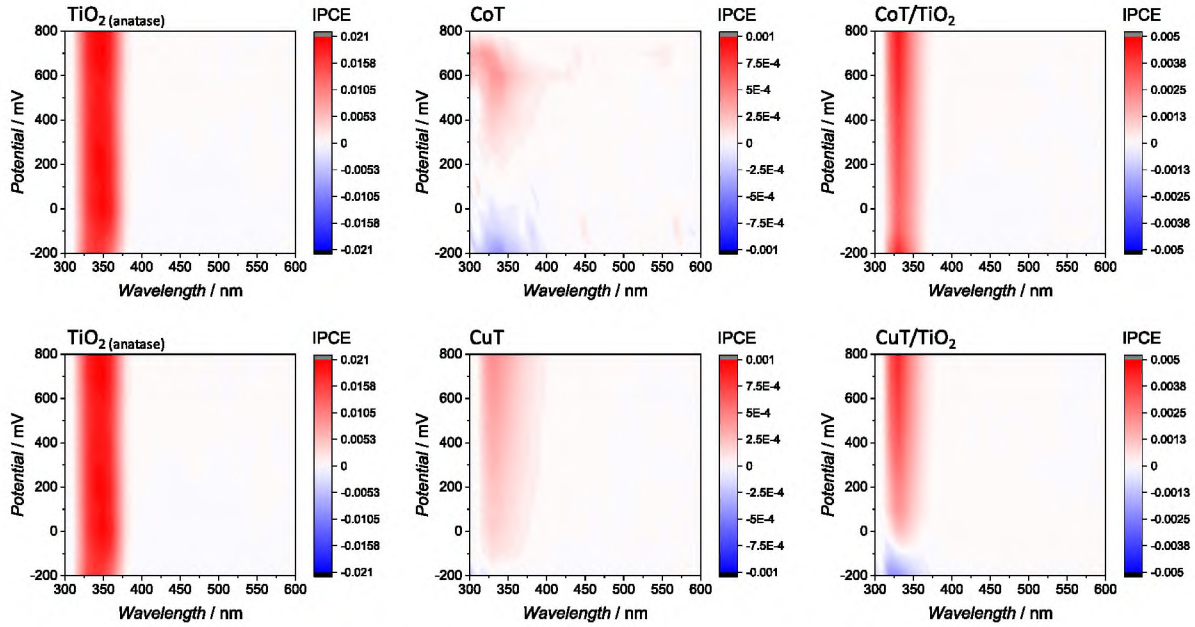

Fig. 6. IPCE maps of TiO_2, CoT, CuT and their mixtures.

successful performance of such junctions. The activity of CuT/TiO_2 compared to pure CuT is only slightly higher. However, it was consistently and reproducibly higher for every point for every sampling time and so is considered significant and points to a higher activity.

Both CoT and CuT have W^{5+} active sites exhibiting the affinity to bonding carbon-containing species [69], which can be beneficial in the CO_2 reduction process, as it can increase substrate adsorption. The higher activity of CuT may originate from the W^{5+} prevalence and presence of Cu, which is also discussed in the literature as an effective center of CO_2 adsorption and reduction [70,71]. The presence of the mentioned sites is advantageous but also leads to surface poisoning (especially with CO and HCHO) and thus inhibiting the reduction of CO_2 over time. Therefore, the stability of photoactivity of CoT/TiO_2 and CuT/TiO_2 was verified in three consecutive runs (**Fig. S6**). For both CoT/TiO_2 and CuT/TiO_2, the activity lowers by *ca.* 50% after three runs, however, in the case of CoT/TiO_2, this drop takes place already during the second run, while for the CuT/TiO_2 the decrease is gradual. These results may indicate severe surface poisoning or photocorrosion – an

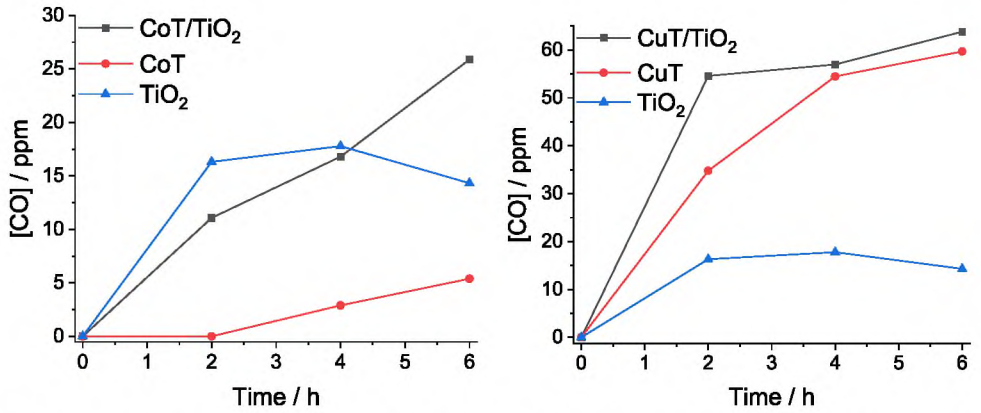

Fig. 7. Plots depicting the changes in the CO concentration during the photocatalytic tests with CoT/TiO_2 (left) and CuT/TiO_2 (right).

explanation of the activity drop would require further examination.

SPV and DOS

For further elucidation of the heterojunctions' formation and mechanisms of their photoactivity, SPV measurements were conducted (Fig. 8). The change in the CPD (ΔCPD) caused by irradiation was presented (the absolute value of CPD, which was the baseline, was subtracted). The change in the CPD is related to the accumulation of net charge on the surface during irradiation which changes the work function of the material. To determine the electrons flow between the materials in the junctions the following approach was adopted – the layer of one material was placed on top of the layer of the other material, *e.g.*, the CoT layer on the top of the TiO_2 layer, and *vice versa* [72,73]. Obtained data indicate that in the case of CoT/TiO_2, the junction is formed which is evident as the change of CPD values compared to the changes of CPD for bare materials under irradiation. However, the electrons flow is possible from CoT to TiO_2 as well as in the opposite direction when the semiconductors are excited as can be seen by the decrease in CPD values both during irradiation periods when the CoT layer is on the top and when the TiO_2 layer is on the top. In the case of CuT/TiO_2 instead, when TiO_2 is on the top, the CPD values are positive, indicating the charge transfer from TiO_2 to CuT. When CuT is placed on top of the TiO_2, the switch from the positive values to negative is observed in the range of main absorption of TiO_2 ($\lambda < 380$), which is related to the transfer of electrons from excited TiO_2 to CuT. When TiO_2 is not excited, the excited CuT may transfer electrons to TiO_2. However, the process is not effective, as a relatively negligible increase of ΔCPD under the 380–400 nm range of light is observed. Such behavior indicates the creation of a higher barrier between CuT and TiO_2 than in CoT and TiO_2.

To determine the reason for the flow of charges indicated by SPV results, the SE-DRS measurements were performed. This technique allows for the estimation of the conduction band edge of examined material by filling the empty electronic states with electrons by applying the negative potential, and therefore, changing the material absorption spectrum. The data are presented as the value of differences between the Kubelka-Munk function at a given wavelength recorded for two subsequent potentials. This value corresponds to the density of states of the material [74]. Fig. 9 presents the results for synthesized materials and TiO_2.

As can be seen, the CB edge for CoT lies at a significantly lower potential than the CB of TiO_2, whereas the CB for CuT almost overlaps with the one of TiO_2. Despite the CuT CB edge lies at a slightly lower potential than the edge of TiO_2 CB, there are some localized states under the CuT CB edge. This finding is in agreement with the literature reports [75,76]. These states should be able to accept electrons from excited TiO_2. It is consistent with SPV measurements that indicate a favourable electron transfer from excited CuT to TiO_2. These outcomes led us to propose different mechanisms of the two heterojunctions' activity (Fig. 10).

Taking into account the photocatalytic tests, it is possible, that the lower activity for CoT in the junction with TiO_2 is the result of the competition between the electron flow directions denoted as $I_{e^-,1}$ (major) and $I_{e^-,2}$ (minor) in Fig. 10. However, such competition would not be observed for the CuT/TiO_2 junction, as the $I_{e^-,1}$ and $I_{e^-,2}$ have the same direction, and the junction can possibly work as the type-I heterojunction or an S-scheme heterojunction making the charge carriers separation more efficient and therefore promoting CO_2 reduction. Taking into account the enhanced activity in CO_2 reduction it can be concluded that CoT/TiO_2 exhibits rather an S-scheme behavior, however, due to the competing, non-negligible $I_{e^-,2}$ current, the classical S-scheme can be considered disturbed.

To exclude the possibility of H_2O oxidation to hydroxyl radicals at the tungstates, additional photocatalytic tests of oxidation of

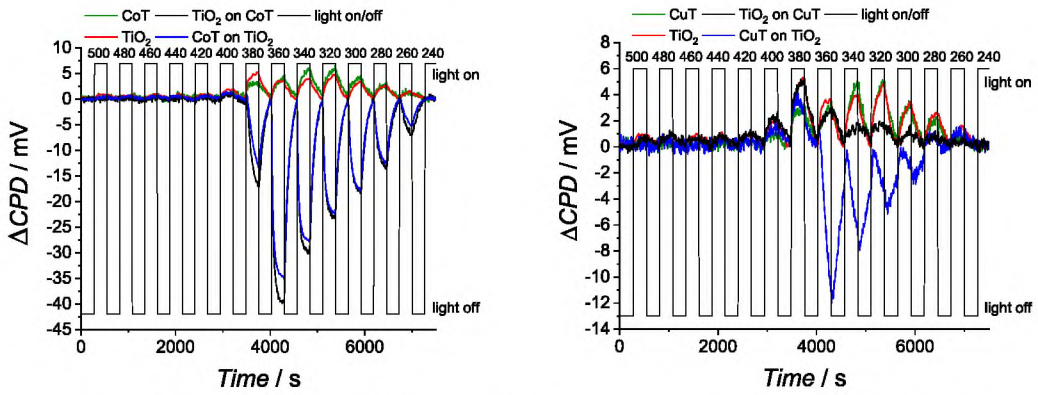

Fig. 8. SPV measurements of bare and layered tungstates and TiO_2: systems with CoT (left) and CuT (right).

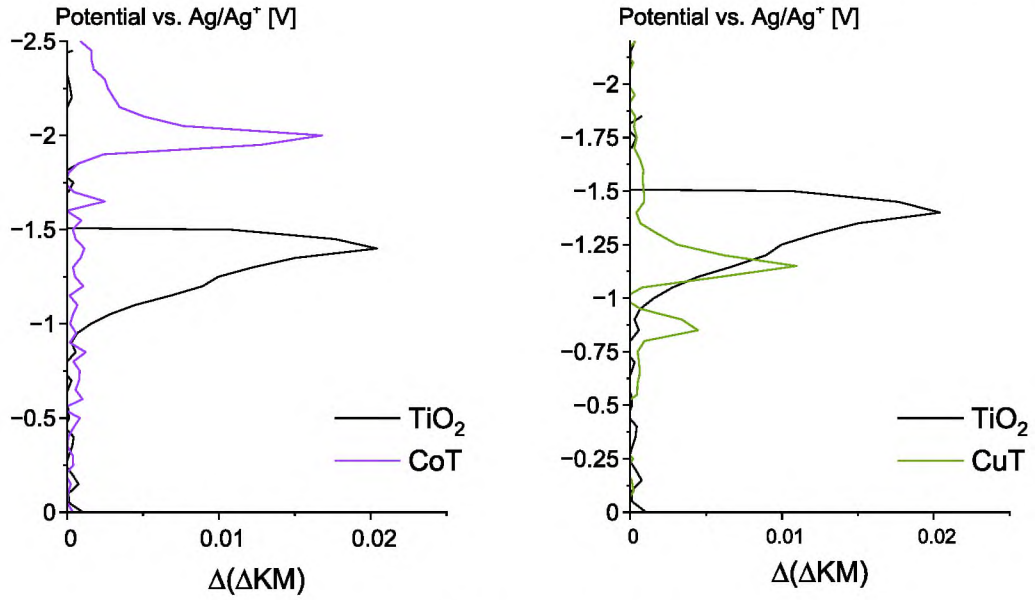

Fig. 9. SE-DRS measurements of TiO_2 compared with CoT (left) and CuT (right).

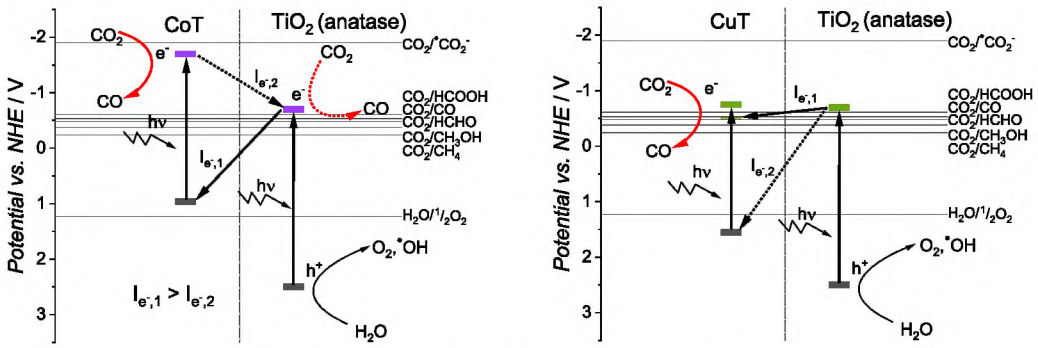

Fig. 10. Mechanisms of heterojunctions photoactivity of CoT/TiO_2 (left) and CuT/TiO_2 (right).

terephthalic acid to hydroxyterephthalic acid were made on bare materials. As expected, TiO_2 exhibits high activity in hydroxyl radical formation, whereas the studied tungstates have no detectable activity (**Fig. S7**). Montini et al. compared selected $MeWO_4$ (Me = Cu^{II}, Co^{II}, Ni^{II}, Zn^{II}) in the photocatalytic degradation of organic dyes and concluded that only $ZnWO_4$ is effective in this process [77], which indicates inefficient hydroxyl radicals formation on $CuWO_4$ and $CoWO_4$. Therefore, in the case of CuT/TiO_2 and CoT/TiO_2 the active site for the H_2O oxidation reaction can be assigned directly to TiO_2, which corroborates with the proposed mechanisms.

Conclusions

Two different materials from the class of tungstates were synthesized and characterized. It was found, that the cation precursor has a strong effect on the resulting material properties. The synthesis conditions enabled achieving a large number of oxygen vacancies and W^{5+} centers that are advantageous in terms of CO_2 bonding and reduction.

Both materials show activity in CO_2 reduction which is enhanced in mixtures with TiO_2. The activity of CuT/TiO_2 turned out to be better than that of CoT/TiO_2 which may be ascribed to lower recombination rates of photogenerated charge carriers and to the presence of a larger number of defects and Cu^{2+} centers active in CO_2 reduction. The differences in the activity of both materials and their mixtures were further elucidated with spectroelectrochemical and surface photovoltage measurements. It was found that depending on the electronic properties of the materials, the height of the barrier differs, determining the type of junction between the materials (here: the disturbed S-scheme and the type-I heterojunction for CoT/TiO_2 and CuT/TiO_2, respectively). In the case of CuT/TiO_2 the transfer in only one direction was observed, whereas for CoT/TiO_2 the charge flow in both directions (*i.e.*, from CoT to TiO_2 and reverse) can take place. Such behavior may disturb the efficient performance of the CoT/TiO_2 system. Therefore, CuT is considered to be a more promising candidate to create useful mixtures with TiO_2 for photocatalytic CO_2 reduction.

Our analysis shows, that it is necessary to examine the nature of the contact between the components and electronic structure of the materials creating the mixtures to establish the possibility of charge carriers flow between them for the correct determination of the junction type.

CRediT authorship contribution statement

Kamil Urbanek: Conceptualization, Data curation, Formal analysis, Investigation, Methodology, Validation, Visualization, Writing – original draft, Writing – review & editing. **Anna Jakimińska:** Conceptualization, Data curation, Formal analysis, Investigation, Methodology, Validation, Visualization, Writing – original draft, Writing – review & editing. **Kaja Spilarewicz:** Conceptualization, Data curation, Formal analysis, Investigation, Methodology, Validation, Visualization, Writing – original draft, Writing – review & editing. **Wojciech Macyk:** Conceptualization, Funding acquisition, Methodology, Supervision, Writing – original draft, Writing – review & editing.

Declaration of Competing Interest

The authors declare that they have no known competing financial interests or personal relationships that could have appeared to influence the work reported in this paper.

Data availability

Data will be made available on request.

Acknowledgments

This work was supported by the National Science Center, Poland, within the Sheng 1 project (2018/30/Q/ST5/00776). The research was partially carried out with the equipment purchased thanks to the financial support of the European Union in the framework of the Polish Smart Growth Operational Programme (contract no. POIR.04.02.00-00-D001/20).

Supplementary materials

Supplementary material associated with this article can be found, in the online version, at doi:10.1016/j.apsadv.2023.100473.

References

[1] P. Dong, G. Hou, X. Xi, R. Shao, F. Dong, WO_3-based photocatalysts: morphology control, activity enhancement and multifunctional applications, Environ. Sci. Nano. 4 (2017) 539–557, https://doi.org/10.1039/C6EN00478D.

[2] O. Samuel, M.H.D. Othman, R. Kamaludin, O. Sinsamphanh, H. Abdullah, M. H. Puteh, T.A. Kurniawan, WO_3–based photocatalysts: a review on synthesis, performance enhancement and photocatalytic memory for environmental applications, Ceram. Int. 48 (2022) 5845–5875, https://doi.org/10.1016/j.ceramint.2021.11.158.

[3] V. Dutta, S. Sharma, P. Raizada, V.K. Thakur, A.A.P. Khan, V. Saini, A.M. Asiri, P. Singh, An overview on WO_3 based photocatalyst for environmental remediation, J. Environ. Chem. Eng. 9 (2021), 105018, https://doi.org/10.1016/j.jece.2020.105018.

[4] H. Wang, L. Zhang, Y. Zhou, S. Qiao, X. Liu, W. Wang, Photocatalytic CO_2 reduction over platinum modified hexagonal tungsten oxide: effects of platinum on forward and back reactions, Appl. Catal. B Environ. 263 (2020), 118331, https://doi.org/10.1016/j.apcatb.2019.118331.

[5] T. Inoue, A. Fujishima, S. Konishi, K. Honda, Photoelectrocatalytic reduction of carbon dioxide in aqueous suspensions of semiconductor powders, Nature 277 (1979) 637–638, https://doi.org/10.1038/277637a0.

[6] N.E. Mendieta-Reyes, A.K. Díaz-García, R. Gómez, Simultaneous electrocatalytic CO_2 reduction and enhanced electrochromic effect at WO_3 nanostructured electrodes in acetonitrile, ACS Catal. 8 (2018) 1903–1912, https://doi.org/10.1021/acscatal.7b03047.

[7] T. Kimura, H. Sunaba, K. Kamata, N. Mizuno, Efficient $[WO_4]^{2-}$-catalyzed chemical fixation of carbon dioxide with 2-aminobenzonitriles to quinazoline-2,4(1 *H,3 H*)-diones, Inorg. Chem. 51 (2012) 13001–13008, https://doi.org/10.1021/ic302110a.

[8] T. Kimura, K. Kamata, N. Mizuno, A bifunctional tungstate catalyst for chemical fixation of CO_2 at atmospheric pressure, Angew. Chem. Int. Ed. 51 (2012) 6700–6703, https://doi.org/10.1002/anie.201203189.

[9] H. Wang, L. Zhang, K. Wang, X. Sun, W. Wang, Enhanced photocatalytic CO_2 reduction to methane over WO_3·0·33H_2O via Mo doping, Appl. Catal. B Environ. 243 (2019) 771–779, https://doi.org/10.1016/j.apcatb.2018.11.021.

[10] S. Sun, M. Watanabe, J. Wu, Q. An, T. Ishihara, Ultrathin WO_3·0·33H_2O nanotubes for CO_2 photoreduction to acetate with high selectivity, J. Am. Chem. Soc. 140 (2018) 6474–6482, https://doi.org/10.1021/jacs.8b03316.

[11] G.A. Niklasson, L. Berggren, A.-L. Larsson, Electrochromic tungsten oxide: the role of defects, Sol. Energy Mater. Sol. Cells. 84 (2004) 315–328, https://doi.org/10.1016/j.solmat.2004.01.045.

[12] S. Huang, Y. Long, S. Ruan, Y.-J. Zeng, Enhanced photocatalytic CO_2 reduction in defect-engineered Z-scheme WO_{3-x}/g-C_3N_4 heterostructures, ACS Omega 4 (2019) 15593–15599, https://doi.org/10.1021/acsomega.9b01969.

[13] S. Tan, Y. Zhao, J. Zhao, Z. Wang, C. Ma, A. Zhao, B. Wang, Y. Luo, J. Yang, J. Hou, CO_2 dissociation activated through electron attachment on the reduced rutile TiO_2(110)-1 × 1 surface, Phys. Rev. B. 84 (2011), 155418, https://doi.org/10.1103/PhysRevB.84.155418.

[14] J. Lee, D.C. Sorescu, X. Deng, Electron-induced dissociation of CO_2 on TiO_2(110), J. Am. Chem. Soc. 133 (2011) 10066–10069, https://doi.org/10.1021/ja204077e.

[15] J.I. Martins, Leaching systems of wolframite and scheelite: a thermodynamic approach, Miner. Process. Extr. Metall. Rev. 35 (2014) 23–43, https://doi.org/10.1080/08827508.2012.757095.

[16] G. Johansson, R. Caminiti, The hydration of tungstate and molybdate ions in aqueous solution, Z. Für Naturforschung A. 41 (1986) 1325–1329, https://doi.org/10.1515/zna-1986-1111.

[17] K. Nassau, L.G. Van Uitert, Preparation of large calcium-tungstate crystals containing paramagnetic ions for maser applications, J. Appl. Phys. 31 (2004) 1508, https://doi.org/10.1063/1.1735881.

[18] K. Nassau, H.J. Levinstein, O.M. Loiacono, Trivalent rare-earth tungstates of the type $M_2(WO_4)_3$, J. Am. Ceram. Soc. 47 (1964) 363–364, https://doi.org/10.1111/j.1151-2916.1964.tb13005.x.

[19] H.D. Abdul kader, I. Sh. Mohammed, S.H. Ammar, Synthesis of recyclablecore/shell $CoFe_2O_4$@$CoWO_4$ photocatalysts for efficient visible-light photocatalytic degradation of environmental pollutants, Environ. Nanotechnol. Monit. Manag. 17 (2022), 100664, https://doi.org/10.1016/j.enmm.2022.100664.

[20] P.A. Shinde, S.C. Jun, Review on Recent Progress in the Development of Tungsten Oxide Based Electrodes for Electrochemical Energy Storage, ChemSusChem 13 (2020) 11–38, https://doi.org/10.1002/cssc.201902071.

[21] K. Hoang, M. Oh, Y. Choi, Electronic structure, polaron formation, and functional properties in transition-metal tungstates, RSC Adv 8 (2018) 4191–4196, https://doi.org/10.1039/C7RA13436C.

[22] J. Ungelenk, M. Speldrich, R. Dronskowski, C. Feldmann, Polyol-mediated low-temperature synthesis of crystalline tungstate nanoparticles MWO_4 (M = Mn, Fe, Co, Ni, Cu, Zn), Solid State Sci 31 (2014) 62–69, https://doi.org/10.1016/j.solidstatesciences.2014.02.020.

[23] P. Chen, H.-Y. He, H_2 evolution from H_2O/H_2O_2/MWO_4 (M = Fe^{2+}, Co^{2+}, Ni^{2+}) systems by photocatalytic reaction, Res. Chem. Intermed. 40 (2014) 1947–1956, https://doi.org/10.1007/s11164-013-1092-5.

[24] B.J. Rani, G. Ravi, S. Ravichandran, V. Ganesh, F. Ameen, A. Al-Sabri, R. Yuvakkumar, Electrochemically active XWO_4 (X = Co, Cu, Mn, Zn) nanostructure for water splitting applications, Appl. Nanosci. 8 (2018) 1241–1258, https://doi.org/10.1007/s13204-018-0780-2.

[25] X.A. López, A.F. Fuentes, M.M. Zaragoza, J.A. Díaz Guillén, J.S. Gutiérrez, A. L. Ortiz, V. Collins-Martínez, Synthesis, characterization and photocatalytic evaluation of MWO_4 (M = Ni, Co, Cu and Mn) tungstates, Int. J. Hydrog. Energy. 41 (2016) 23312–23317, https://doi.org/10.1016/j.ijhydene.2016.10.117.

[26] U.M. García-Pérez, A. Martínez-de la Cruz, J. Peral, Transition metal tungstates synthesized by co-precipitation method: basic photocatalytic properties, Electrochim. Acta 81 (2012) 227–232, https://doi.org/10.1016/j.electacta.2012.07.045.

[27] X. Du, Z. Dai, Y. Wang, X. Han, X. Zhang, Facile synthesis of MWO_4 (M=Co, Ni, Zn and Cu) nanoarrays for efficient urea oxidation, Int. J. Hydrog. Energy. 47 (2022) 8875–8882, https://doi.org/10.1016/j.ijhydene.2021.12.244.

[28] B. Li, F. Wei, B. Su, Z. Guo, Z. Ding, M.-Q. Yang, S. Wang, Mesoporous cobalt tungstate nanoparticles for efficient and stable visible-light-driven photocatalytic CO_2 reduction, Mater. Today Energy. 24 (2022), 100943, https://doi.org/10.1016/j.mtener.2022.100943.

[29] H. Farsi, S. Moghiminia, M. Raygan, E. Dana, S. Hosseini, M. Behforooz, T. Zubkov, I.V. Lightcap, Z. Li, Nanostructured tungstate-derived copper for hydrogen evolution reaction and electroreduction of CO_2 in sodium hydroxide solutions, J. Phys. Chem. C. 123 (2019) 25941–25948, https://doi.org/10.1021/acs.jpcc.9b07133.

[30] N. Güy, K. Atacan, M. Özacar, Rational construction of p-n-p CuO/CdS/$CoWO_4$ S-scheme heterojunction with influential separation and directional transfer of interfacial photocarriers for boosted photocatalytic H2 evolution, Renew. Energy. 195 (2022) 107–120, https://doi.org/10.1016/j.renene.2022.05.171.

[31] P. Taneja, S. Sharma, A. Umar, S.K. Mehta, A.O. Ibhadon, S.K. Kansal, Visible-light driven photocatalytic degradation of brilliant green dye based on cobalt tungstate ($CoWO_4$) nanoparticles, Mater. Chem. Phys. 211 (2018) 335–342, https://doi.org/10.1016/j.matchemphys.2018.02.041.

[32] A. Sarwar, A. Razzaq, M. Zafar, I. Idrees, F. Rehman, W.Y. Kim, Copper tungstate ($CuWO_4$)/graphene quantum dots (GQDs) composite photocatalyst for enhanced degradation of phenol under visible light irradiation, Results Phys 45 (2023), 106253, https://doi.org/10.1016/j.rinp.2023.106253.

[33] Q. Niu, Q. Chen, G. Huang, L. Li, Y. He, J. Bi, Build-in electric field in $CuWO_4$/covalent organic frameworks S-scheme photocatalysts steer boosting charge transfer for photocatalytic CO_2 reduction, J. Colloid Interface Sci. 643 (2023) 102–114, https://doi.org/10.1016/j.jcis.2023.04.013.

[34] N. Jatav, A. Shrivastava, A. Kumar De, I. Sinha, Experimental and molecular dynamics investigations on Z-scheme visible light Ag_3PO_4/$CuWO_4$ photocatalysts for antibiotic degradation, J. Environ. Chem. Eng. 10 (2022), 107975, https://doi.org/10.1016/j.jece.2022.107975.

[35] P. Raizada, S. Sharma, A. Kumar, P. Singh, A.A. Parwaz Khan, A.M. Asiri, Performance improvement strategies of $CuWO_4$ photocatalyst for hydrogen generation and pollutant degradation, J. Environ. Chem. Eng. 8 (2020), 104230, https://doi.org/10.1016/j.jece.2020.104230.

[36] W. Xu, Q. Zhang, X. Kang, H. Guo, J. Song, L. Wang, Study on visible-light photocatalytic performance of $CuWO_4$ modified by boron nitride, Mater. Lett. 330 (2023), 133357, https://doi.org/10.1016/j.matlet.2022.133357.

[37] L. Chang, Y. Pu, P. Jing, J. Ji, X. Wei, B. Cao, Y. Yu, S. Xu, H. Xie, Z-Scheme $CuWO_4$/BiOCl photocatalysts with oxygen vacancy as electron mediator for boosted photocatalytic degradation of norfloxacin, Surf. Interfaces. 31 (2022), 102010, https://doi.org/10.1016/j.surfin.2022.102010.

[38] H. Chen, Y. Xu, Photocatalytic organic degradation over W-rich and Cu-rich $CuWO_4$ under UV and visible light, RSC Adv 5 (2015) 8108–8113, https://doi.org/10.1039/C4RA13952F.

[39] T.T. My Hang, N.H. Thao Vy, N.T. Hanh, T.-D. Pham, L.T. Hoang Yen, Facile synthesis of copper tungstate ($CuWO_4$) for novel photocatalytic degradation of

tetracycline under visible light, Sustain. Chem. Pharm. 21 (2021), 100407, https://doi.org/10.1016/j.scp.2021.100407.
[40] S.M. Pourmortazavi, M. Rahimi-Nasrabadi, M. Khalilian-Shalamzari, H.R. Ghaeni, S.S. Hajimirsadeghi, Facile chemical synthesis and characterization of copper tungstate nanoparticles, J. Inorg. Organomet. Polym. Mater. 24 (2014) 333–339, https://doi.org/10.1007/s10904-013-9970-2.
[41] L.P. Dorfman, D.L. Houck, M.J. Scheithauer, J.N. Dann, H.O. Fassett, Solid-phase synthesis of cupric tungstate, J. Mater. Res. 16 (2001) 1096–1102, https://doi.org/10.1557/JMR.2001.0152.
[42] A.K. Basu, F.R. Sale, Copper-tungsten composite powders by the hydrogen reduction of copper tungstate, J. Mater. Sci. 13 (1978) 2703–2711, https://doi.org/10.1007/BF02402759.
[43] F. Shahdost-Fard, S. Faridfar, A.H. Keihan, M. Aghaei, I. Petrenko, F. Ahmadi, H. Ehrlich, M. Rahimi-Nasrabadi, Applicability of a green nanocomposite consisted of spongin decorated $Cu_2WO_4(OH)_2$ and AgNPs as a high-performance aptasensing platform in staphylococcus aureus detection, Biosensors 13 (2023) 271, https://doi.org/10.3390/bios13020271.
[44] X. Bai, Z. Fu, X. Ma, Z. Zhang, J. Fan, E. Liu, J. Li, Hydrophilic regulated photocatalytic converting phenol selectively over S-scheme $CuWO_4/TiO_2$, J. Clean. Prod. 369 (2022), 133099, https://doi.org/10.1016/j.jclepro.2022.133099.
[45] M.E. Malefane, P.J. Mafa, M. Managa, T.T.I. Nkambule, A.T. Kuvarega, Understanding the principles and applications of dual Z-scheme heterojunctions: how far can we go? J. Phys. Chem. Lett. 14 (2023) 1029–1045, https://doi.org/10.1021/acs.jpclett.2c03387.
[46] J.E. Yourey, B.M. Bartlett, Electrochemical deposition and photoelectrochemistry of $CuWO_4$, a promising photoanode for water oxidation, J. Mater. Chem. 21 (2011) 7651–7660, https://doi.org/10.1039/C1JM11259G.
[47] X. Bao, X. Wang, X. Li, L. Qin, S. Han, S.-Z. Kang, $CuWO_{4-x}$ nanoparticles incorporated brookite TiO_2 porous nanospheres: preparation and dramatic photocatalytic activity for light driven H_2 generation, Mater. Res. Bull. 136 (2021), 111171, https://doi.org/10.1016/j.materresbull.2020.111171.
[48] U. Bharagav, N.R. Reddy, V.N. Rao, P. Ravi, M. Sathish, M.V. Shankar, M. M. Kumari, $CuWO_4$ as a novel Z-scheme partner to construct TiO_2 based stable and efficient heterojunction for photocatalytic hydrogen generation, Int. J. Hydrog. Energy. 47 (2022) 40391–40406, https://doi.org/10.1016/j.ijhydene.2022.07.155.
[49] I.V. Lukiyanchuk, M.S. Vasilyeva, N.I. Steblevskaya, M.V. Belobeletskaya, A. Yu. Ustinov, V.V. Tkachev, Yu.B. Budnikova, A.A. Rybalka, K.A. Sergeeva, TiO_2-WO_3-$Eu_2(WO_4)_3$ film heterostructures: synthesis, luminescent, optoelectronic and photocatalytic properties, J. Alloys Compd. 955 (2023), 170318, https://doi.org/10.1016/j.jallcom.2023.170318.
[50] L. Collado, M. Gomez-Mendoza, M. García-Tecedor, F.E. Oropeza, A. Reynal, J. R. Durrant, D.P. Serrano, V.A. de la Peña O'Shea, Towards the improvement of methane production in CO_2 photoreduction using Bi_2WO_6/TiO_2 heterostructures, Appl. Catal. B Environ. 324 (2023), 122206, https://doi.org/10.1016/j.apcatb.2022.122206.
[51] C. Feng, Q. Gu, J. Rong, Q. Liang, M. Zhou, X. Li, S. Xu, Z. Li, Porous dual Z-scheme InOOH/RCN/$CoWO_4$ heterojunction with enhanced photothermal-photocatalytic properties towards norfloxacin degradation, Sep. Purif. Technol. 308 (2023), 122890, https://doi.org/10.1016/j.seppur.2022.122890.
[52] P. Makuła, M. Pacia, W. Macyk, How to correctly determine the band gap energy of modified semiconductor photocatalysts based on UV–vis spectra, J. Phys. Chem. Lett. 9 (2018) 6814–6817, https://doi.org/10.1021/acs.jpclett.8b02892.
[53] A. Altomare, N. Corriero, C. Cuocci, A. Falcicchio, A. Moliterni, R. Rizzi, QUALX2.0: a qualitative phase analysis software using the freely available database POW_COD, J. Appl. Crystallogr. 48 (2015) 598–603, https://doi.org/10.1107/S1600576715002319.
[54] S. Gražulis, D. Chateigner, R.T. Downs, A.F.T. Yokochi, M. Quirós, L. Lutterotti, E. Manakova, J. Butkus, P. Moeck, A.Le Bail, Crystallography Open Database – an open-access collection of crystal structures, J. Appl. Crystallogr. 42 (2009) 726–729, https://doi.org/10.1107/S0021889809016690.
[55] S. Gražulis, A. Daškevič, A. Merkys, D. Chateigner, L. Lutterotti, M. Quirós, N. R. Serebryanaya, P. Moeck, R.T. Downs, A.Le Bail, Crystallography Open Database (COD): an open-access collection of crystal structures and platform for world-wide collaboration, Nucleic Acids Res 40 (2012) D420–D427, https://doi.org/10.1093/nar/gkr900.
[56] M. Quirós, S. Gražulis, S. Girdzijauskaitė, A. Merkys, A. Vaitkus, Using SMILES strings for the description of chemical connectivity in the crystallography open database, J. Cheminformatics. 10 (2018) 23, https://doi.org/10.1186/s13321-018-0279-6.
[57] A. Vaitkus, A. Merkys, S. Gražulis, Validation of the crystallography open database using the crystallographic information framework, J. Appl. Crystallogr. 54 (2021) 661–672, https://doi.org/10.1107/S1600576720016532.
[58] H. Kisch, Semiconductor Photocatalysis, Wiley-VCH, 2014.
[59] L. Zhen, W.-S. Wang, C.-Y. Xu, W.-Z. Shao, L.-C. Qin, A facile hydrothermal route to the large-scale synthesis of $CoWO_4$ nanorods, Mater. Lett. 62 (2008) 1740–1742, https://doi.org/10.1016/j.matlet.2007.09.076.
[60] W. Cheng, K. Tang, Z. Liu, J. Sheng, Y. Qi, Template-free synthesis of monodisperse $Cu_2WO_4(OH)_2$ round and elliptical hollow spheres with a ligand-assisted dissolution process, Chem. Commun. (2009) 7185–7187, https://doi.org/10.1039/B914086G.
[61] E.L.S. Souza, J.C. Sczancoski, I.C. Nogueira, M.A.P. Almeida, M.O. Orlandi, M.S. Li, R.A.S. Luz, M.G.R. Filho, E. Longo, L.S. Cavalcante, Structural evolution, growth mechanism and photoluminescence properties of $CuWO_4$ nanocrystals, Ultrason. Sonochem. 38 (2017) 256–270, https://doi.org/10.1016/j.ultsonch.2017.03.007.
[62] Cuprotungstite, (n.d.). https://www.mindat.org/min-1194.html (accessed July 13, 2023).
[63] L. Kihlborg, E. Gebert, $CuWO_4$, a distorted Wolframite-type structure, Acta Crystallogr. Sect. B. 26 (1970) 1020–1026, https://doi.org/10.1107/S0567740870003515.
[64] C. Huang, D. Wang, W. Zhang, S.J. Yoo, X. Zhou, K. Song, Z. Chen, X. Zou, N. Yue, Z. Wang, J.-G. Kim, W. Zheng, Substitution-triggered broken symmetry of cobalt tungstate boosts redox kinetics in pseudocapacitive storage, Cell Rep. Phys. Sci. 3 (2022), 101115, https://doi.org/10.1016/j.xcrp.2022.101115.
[65] T.H. Fleisch, G.J. Mains, An XPS study of the UV reduction and photochromism of MoO_3 and WO_3, J. Chem. Phys. 76 (1982) 780–786, https://doi.org/10.1063/1.443047.
[66] M. Fantauzzi, F. Secci, M.S. Angotzi, C. Passiu, C. Cannas, A. Rossi, Nanostructured spinel cobalt ferrites: fe and Co chemical state, cation distribution and size effects by X-ray photoelectron spectroscopy, RSC Adv 9 (2019) 19171–19179, https://doi.org/10.1039/C9RA03488A.
[67] S.M. AlShehri, J. Ahmed, T. Ahamad, P. Arunachalam, T. Ahmad, A. Khan, Bifunctional electro-catalytic performances of $CoWO_4$ nanocubes for water redox reactions (OER/ORR), RSC Adv. 7 (2017) 45615–45623, https://doi.org/10.1039/C7RA07256B.
[68] A. Paul Chowdhury, B.H. Shambharkar, Synthesis and photocatalytic properties of sunlight-responsive BiOBr–$CoWO_2$ heterostructured nanocomposites, Appl. Organomet. Chem. 34 (2020) e5436, https://doi.org/10.1002/aoc.5436.
[69] Y. Feng, C. Wang, P. Cui, C. Li, B. Zhang, L. Gan, S. Zhang, X. Zhang, X. Zhou, Z. Sun, K. Wang, Y. Duan, H. Li, K. Zhou, H. Huang, A. Li, C. Zhuang, L. Wang, Z. Zhang, X. Han, Ultrahigh photocatalytic CO_2 reduction efficiency and selectivity manipulation by single-tungsten-atom oxide at the atomic step of TiO_2, Adv. Mater. 34 (2022), 2109074, https://doi.org/10.1002/adma.202109074.
[70] Y. Wang, Z. Wang, D. Wang, J. Mao, C. Zhang, Y. Zhang, Revealing the doping effect of Cu^{2+} on $SrSnO_3$ perovskite oxides for CO_2 electroreduction, ChemElectroChem 9 (2022), e202200635, https://doi.org/10.1002/celc.202200635.
[71] Q. Wang, Q. Yan, Y. Zhao, J. Ren, N. Ai, Preparation of amine-modified Cu-Mg-Al LDH composite photocatalyst, Nanomaterials 12 (2022) 127, https://doi.org/10.3390/nano12010127.
[72] A. Jakimińska, K. Spilarewicz, W. Macyk, Phototransformations of TiO_2/Ag_2O composites and their influence on photocatalytic water splitting accompanied by methanol photoreforming, Nanoscale Adv. 5 (2023) 1926–1935, https://doi.org/10.1039/D2NA00910B.
[73] K. Urbanek, K. Spilarewicz, J. Yu, W. Macyk, Photocatalytic reduction of CO_2 at (SnO_2, Fe_3O_4)/TiO_2 composite, Mater. Today Sustain. 22 (2023), 100386, https://doi.org/10.1016/j.mtsust.2023.100386.
[74] M. Kobielusz, K. Pilarczyk, E. Świętek, K. Szaciłowski, W. Macyk, Spectroelectrochemical analysis of TiO_2 electronic states – implications for the photocatalytic activity of anatase and rutile, Catal. Today. 309 (2018) 35–42, https://doi.org/10.1016/j.cattod.2017.11.013.
[75] J.E. Yourey, K.J. Pyper, J.B. Kurtz, B.M. Bartlett, Chemical stability of $CuWO_4$ for photoelectrochemical water oxidation, J. Phys. Chem. C. 117 (2013) 8708–8718, https://doi.org/10.1021/jp402048b.
[76] K.J. Pyper, J.E. Yourey, B.M. Bartlett, Reactivity of $CuWO_4$ in photoelectrochemical water oxidation is dictated by a midgap electronic state, J. Phys. Chem. C. 117 (2013) 24726–24732, https://doi.org/10.1021/jp408434v.
[77] T. Montini, V. Gombac, A. Hameed, L. Felisari, G. Adami, P. Fornasiero, Synthesis, characterization and photocatalytic performance of transition metal tungstates, Chem. Phys. Lett. 498 (2010) 113–119, https://doi.org/10.1016/j.cplett.2010.08.026.